



Deposition of Composite LSCF-SDC and SSC-SDC Cathodes by Axial-Injection Plasma Spraying

Jeffrey Harris, Musab Qureshi, and Olivera Kesler

(Submitted September 15, 2011; in revised form December 22, 2011)

The performance of solid oxide fuel cell cathodes can be improved by increasing the number of electrochemical reaction sites, by controlling microstructures, or by using composite materials that consist of an ionic conductor and a mixed ionic and electronic conductor. LSCF ($\text{La}_{0.6}\text{Sr}_{0.4}\text{Co}_{0.2}\text{Fe}_{0.8}\text{O}_{3-\delta}$) and SSC ($\text{Sm}_{0.5}\text{Sr}_{0.5}\text{CoO}_3$) cathodes were manufactured by axial-injection atmospheric plasma spraying, and composite cathodes were fabricated by mixing SDC ($\text{Ce}_{0.8}\text{Sm}_{0.2}\text{O}_{1.9}$) into the feedstock powders. The plasma power was varied by changing the proportion of nitrogen in the plasma gas. The microstructures of cathodes produced with different plasma powers were characterized by scanning electron microscopy and gas permeation measurements. The deposition efficiencies of these cathodes were calculated based on the mass of the sprayed cathode. Particle surface temperatures were measured in-flight to enhance understanding of the relationship between spray parameters, microstructure, and deposition efficiency.

Keywords atmospheric plasma spray, composite cathode, deposition efficiency, LSCF, perovskite, solid oxide fuel cell, SSC

1. Introduction

Solid oxide fuel cells (SOFCs) are devices that efficiently convert chemical energy into electrical energy and heat. SOFCs are well suited for stationary power generation, where the overall system efficiency can be maximized in a combined heat and power (CHP) system. SOFCs are particularly attractive because they have the ability to use a variety of currently available fuels and because the fuel and air streams are physically separated, thus facilitating carbon capture and storage.

SOFCs are typically manufactured by wet-ceramic processes; however, plasma spray processes have become attractive because they facilitate the use of metallic

supports. Metal-supported SOFCs can be more mechanically robust than electrode-supported cells, and are considerably less expensive than all-ceramic cells because of lower materials costs. Furthermore, plasma spraying has emerged as an attractive manufacturing process because it is scalable for both low-volume and high-volume production.

$\text{La}_{0.6}\text{Sr}_{0.4}\text{Co}_{0.2}\text{Fe}_{0.8}\text{O}_{3-\delta}$ (LSCF) and composites of LSCF and doped ceria have emerged as leading cathode materials for intermediate temperature (600–800 °C) SOFCs (Ref 1–4). Several studies have shown that cathode performance can be increased with the addition of ceria doped with samaria or gadolinia (Ref 2–4). These composite cathodes have higher ionic conductivity and more potential electrochemical reaction sites than single-phase LSCF cathodes. The fabrication of LSCF cathodes by plasma spraying has been reported in several studies (Ref 5–10), and we have previously defined the window of suitable parameters for plasma spraying LSCF (Ref 10). However, plasma spraying a composite cathode can be challenging due to the large difference between the melting temperatures of LSCF and doped ceria. We first demonstrated the feasibility of fabricating such composites by axially feeding a heterogeneous mixture of LSCF and samaria-doped ceria (SDC) into the plasma (Ref 11).

SSC has emerged as a leading cathode material for lower temperature (650 °C) SOFCs (Ref 12–14). Forming a composite cathode with SDC is not known to increase electrochemical performance, but it helps to prevent the cathode from densifying during operation (Ref 14, 15). Previously, only one study has attempted to fabricate SSC cathodes by solution precursor plasma spraying (SPPS); the electrochemical performance of these cathodes, however, was limited due to the presence of undesired phases (Ref 16). In contrast, we have reported low polarization resistances in cathodes fabricated from dry powder by atmospheric plasma spraying (APS) (Ref 17), and in the

This article is an invited paper selected from presentations at the 2011 International Thermal Spray Conference and has been expanded from the original presentation. It is simultaneously published in *Thermal Spray 2011: Proceedings of the International Thermal Spray Conference*, Hamburg, Germany, September 27–29, 2011, Basil R. Marple, Arvind Agarwal, Margaret M. Hyland, Yuk-Chiu Lau, Chang-Jiu Li, Rogerio S. Lima, and André McDonald, Ed., ASM International, Materials Park, OH, 2011.

Jeffrey Harris, Musab Qureshi, and Olivera Kesler, Department of Mechanical and Industrial Engineering, University of Toronto, 5 King's College Road, Toronto, ON, Canada. Contact e-mails: kesler@mie.utoronto.ca and jharris@mie.utoronto.ca.

present study, we discuss the strategies used to minimize undesired phases and to control microstructures.

2. Experimental Procedure

2.1 Feedstock Preparation

Plasma spray feedstock consisted of spherical spray-dried agglomerated powders of $\text{La}_{0.6}\text{Sr}_{0.4}\text{Co}_{0.2}\text{Fe}_{0.8}\text{O}_{3-\delta}$ (LSCF), $\text{Ce}_{0.8}\text{Sm}_{0.2}\text{O}_{1.9}$ (SDC), and $\text{Sm}_{0.5}\text{Sr}_{0.5}\text{CoO}_3$ (SSC) (Inframat Advanced Materials, CT, USA). The LSCF and SDC powders were calcined for 5.5 h at 1238 and 1200 °C, respectively. Two SSC feedstock powders were prepared: one was calcined at 1000 °C (herein referred to as SSC1000) and the other was calcined at 1050 °C (herein referred to as SSC1050) for 5.5 h. The microstructures of these SSC powders are shown in Fig. 1. Each powder was sieved into a $-45+32\ \mu\text{m}$ size fraction, and the d_{50} particle sizes by volume, measured by laser light scattering, were 37.7, 31.2, and 34.8 μm for LSCF, SDC, and SSC, respectively.

2.2 Plasma Spraying

Coatings were fabricated using axial-injection plasma spraying at atmospheric pressure and using a Northwest

Mettech Axial III Series 600 torch (Northwest Mettech Corporation, North Vancouver, BC). This torch contains an axial feedstock injector in the centre of three converging plasma arcs; thus, the feedstock powders are directly injected into the hot core of the plasma jet. Plasma gases consisted of nitrogen-argon mixtures, and the plasma power was varied by changing the composition of the gas mixture. The total plasma gas flow rate was 200 slpm, and the arc current was 150 A per electrode pair (for a total of 450 A). The particle surface temperature and velocity distributions were measured using a DPV2000 system (Tecnar, St. Bruno, QC). Cathodes were plasma sprayed onto 25.4 mm diameter porous ferritic stainless steel discs using a robot that manipulated the torch with a peak speed of 0.60 m/s.

2.3 Characterization

The plasma spray deposition efficiency (DE) was calculated by dividing the coating mass by the amount of feedstock material fed to the substrate. Using the torch speed and raster pattern, the amount of time that the centre axis of the plasma plume was in front of the substrate was calculated, and this time was multiplied by the calibrated mass flow rate of powder to estimate the amount of feedstock material fed to the substrate. The phases present in the SSC coatings were identified using x-ray diffraction. Previously, we had investigated the relationship between plasma spray parameters and the phases present in LSCF coatings, and the plasma spray parameters used in the present study were previously shown to produce LSCF coatings with no measurable undesired phases (Ref 10).

Coating microstructures were qualitatively evaluated using scanning electron microscopy, and coating thicknesses were measured from these micrographs using image analysis. The gas transport properties of cathodes were quantitatively measured by forced flow experiments: pressure differences up to 6.89 kPa were incrementally applied across coatings on substrates, and the mass flow rates of air through the coatings were measured, as shown in Fig. 2. The pressure was applied to the coating over a projected area of 0.866 cm^2 . The relationship between pressure difference and mass flow rate is linear, as per Darcy's Law. The slopes of mass flow per unit area versus pressure difference (referred to here as "permeation rates") are measures of the gas transport properties of the materials tested. When the permeation rates are higher,

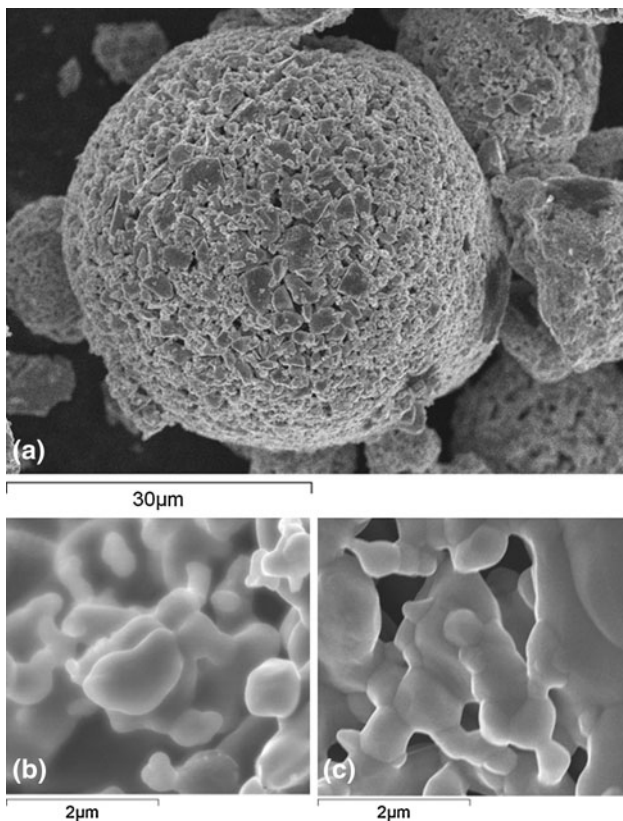


Fig. 1 SSC feedstock: (a) agglomerate of feedstock as-received, (b) high magnification of SSC1000 agglomerate, and (c) high magnification of SSC1050 agglomerate

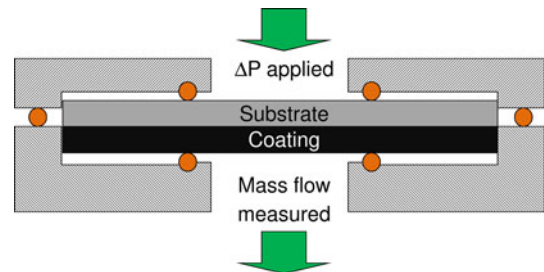


Fig. 2 Characterization apparatus to measure gas transport

oxygen can reach reaction sites more easily, and therefore mass transport overpotentials will be lower. The permeation rate is directly proportional to the porosity, and also depends on the coating thickness and microstructure.

3. Results and Discussion

3.1 Properties of LSCF-Based Cathodes

To understand the relationships between process parameters and coating properties, single-phase LSCF cathodes were fabricated using argon/nitrogen plasmas. The plasma power was varied by changing the plasma gas composition: LSCF coatings were made using plasmas containing 20, 30, 40, 50, and 60% nitrogen (balance argon), resulting in torch powers of 46.0, 52.6, 55.7, 61.5, and 66.3 kW, respectively.

The particle surface temperatures and deposition efficiencies of these coatings are shown in Fig. 3. Notably, the deposition efficiency and mean particle surface temperature increased steeply when the plasma torch power was increased from 53 to 56 kW. It is believed that the surface was above the melting temperature in most particles in the more powerful plasmas; therefore, more particles adhered to the substrate and the deposition efficiency was higher than in the less powerful plasmas. Such high deposition efficiencies (i.e. >80%) are comparable with values reported in other studies using axial-injection plasma spraying (Ref 18, 19). Since cost is a major barrier to the adoption of SOFC technology, it is highly desirable to minimize material loss during plasma spraying by using a process with high deposition efficiency. Therefore, it is desirable to deposit LSCF when the particle surface

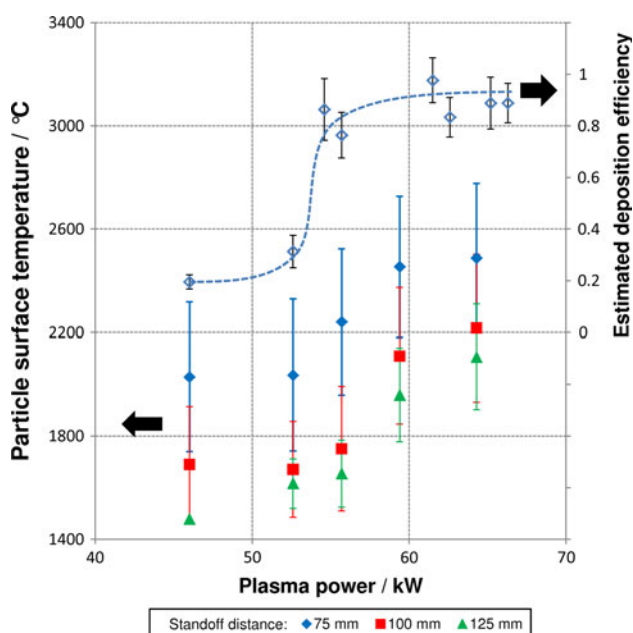


Fig. 3 In-flight temperature measurements and deposition efficiencies of LSCF

temperature is greater than ~ 2200 °C. Overspray, the amount of material not delivered to the substrate, can be decreased by increasing the size of the fuel cells and by using a robot with a higher acceleration and deceleration rate, while the deposition efficiency is characteristic of the deposition process, regardless of the geometry of the substrate or the robot acceleration capacity.

Micrographs of the surfaces of LSCF coatings fabricated with 60, 50, 40, and 30% nitrogen plasmas (balance argon) are shown in Fig. 4. Coatings produced with 20% nitrogen could not be imaged; the coatings wiped off the substrate easily due to poor adhesion. The coatings produced with high deposition efficiencies (60, 50, and 40% nitrogen plasmas) appear to have a substantial amount of melted material. More powerful plasmas resulted in coatings with coarser microstructures, likely due to a greater amount of melting in the plasma. Conversely, the coating produced with a 30% nitrogen plasma appears to have minimal melted material; the fine structure of the spray dried feedstock is almost entirely preserved in the coating. Such a fine microstructure may be desirable for increasing electrochemical activity in the cathode; therefore, excessively powerful plasmas should be avoided. However, a fine structure produced in low plasma powers may have interfaces with higher contact resistance due to worse adhesion than coatings produced with higher power,

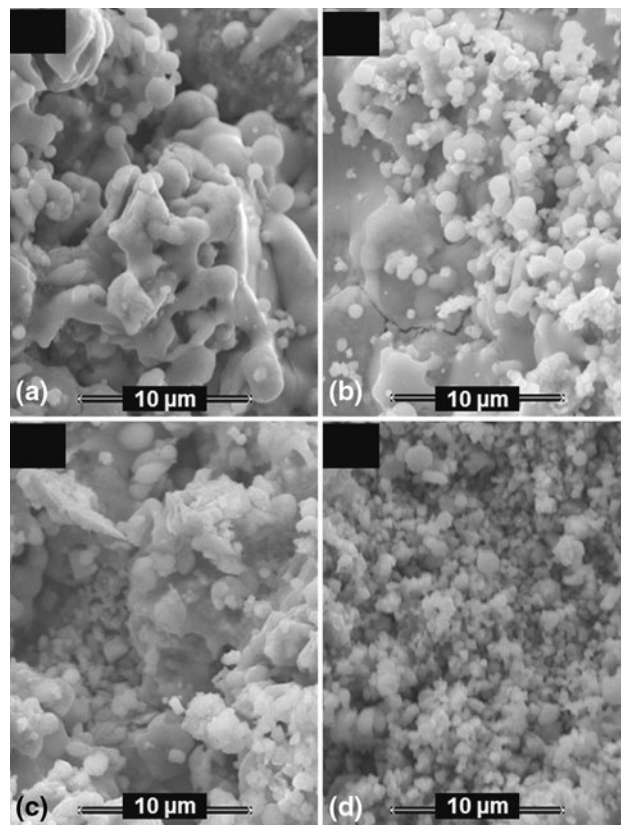


Fig. 4 The surface of LSCF coatings produced with plasmas containing (a) 60%, (b) 50%, (c) 40%, and (d) 30% nitrogen (balance argon) fabricated at 75 mm stand-off distance

so electrochemical testing is needed to determine the best trade-off between high surface area and low contact resistance.

Composite LSCF-SDC cathodes were manufactured from a heterogeneous feedstock mixture containing 60 wt.% LSCF and 40 wt.% SDC. Cathodes in symmetrical cells were manufactured with 53 and 67 kW plasmas, and are shown in Fig. 5. The coating thicknesses clearly show the difference in deposition efficiency; the cathode made with the 53 kW plasma has a thickness of $14 \pm 5 \mu\text{m}$ and a low deposition efficiency of 18%, whereas the cathode made with the 67 kW plasma has a thickness of $61 \pm 10 \mu\text{m}$ and a higher deposition efficiency of 75%. These deposition efficiencies are slightly lower than those of single-phase LSCF because SDC melts at a higher temperature than LSCF. Also, as expected, the permeation rates are significantly different for the two different cathodes: the thin cathode has a permeation rate of $4.20 \text{ sccm/cm}^2/\text{kPa}$, whereas the thicker cathode has a permeation rate of $2.02 \text{ sccm/cm}^2/\text{kPa}$.

Additionally, composite LSCF-SDC coatings adhered poorly to the substrate when intermediate plasma powers ($\sim 56 \text{ kW}$) were used. Since SDC has a higher melting temperature than LSCF, it is likely that a higher particle surface temperature is needed for the feedstock to adhere to the substrate. With a higher temperature, a greater amount of LSCF is melted upon impact, and this material could cement non-melted SDC particles into the coating. As shown in Fig. 5(b), the cathode indeed consists of regions formed from molten feedstock and other regions where much of the structure from the spray dried feedstock was retained.

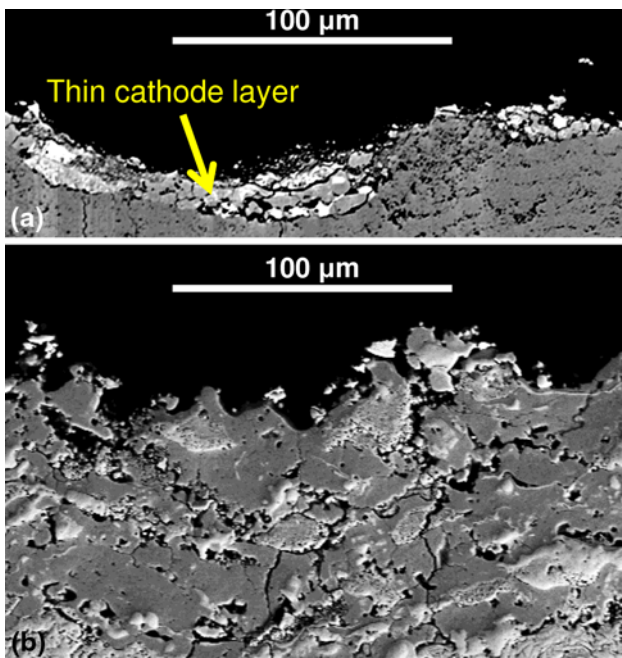


Fig. 5 LSCF-SDC cathodes produced with (a) 53 kW and (b) 67 kW plasmas

3.2 Properties of SSC-Based Cathodes

SSC coatings were fabricated using 43.7, 49.5, 62.4, and 73.2 kW plasmas from SSC1000 feedstock. With the 43.7 and 49.5 kW plasmas, the SSC material (ICDD PDF #00-053-112) slightly decomposed into SrCoO_3 (ICDD PDF # 00-039-1084) and SmCoO_3 (ICDD PDF # 00-025-1071), as visible in the x-ray diffraction patterns in Fig. 6. In these patterns, it appears that decomposition increased when the power was increased from 43.7 kW to 49.6 kW because the relative intensities of the SrCoO_3 and SmCoO_3 phase peaks increased compared to the main SSC peak. However, it is difficult to quantitatively deconvolute the pattern to quantify the fraction of each phase because the primary SSC, SrCoO_3 , and SmCoO_3 peaks are very close together. When the more powerful 62.4 and 73.2 kW plasmas were used, the SrCoO_3 peaks were smaller, and an additional peak at $2\theta = 30^\circ$ was observed, corresponding to SrO (ICDD PDF # 00-001-0886). This result suggests an additional decomposition mechanism, in which the perovskite phase further breaks down into at least one binary oxide. This phenomenon has previously been observed when other perovskite cathode materials were plasma sprayed: LSCF (Ref 10) and LSM (Ref 20) have been found to decompose in plasmas with excessive power, with the perovskite A-site cation (La^{3+}) forming a binary oxide (La_2O_3). In the present work, both the SrO and the SmCoO_3 peaks are largest in the coating fabricated with a 73.2 kW plasma, indicating a greater extent of decomposition with a more powerful plasma. Figure 7 shows backscattered electron cross section micrographs of SSC coatings that were plasma sprayed

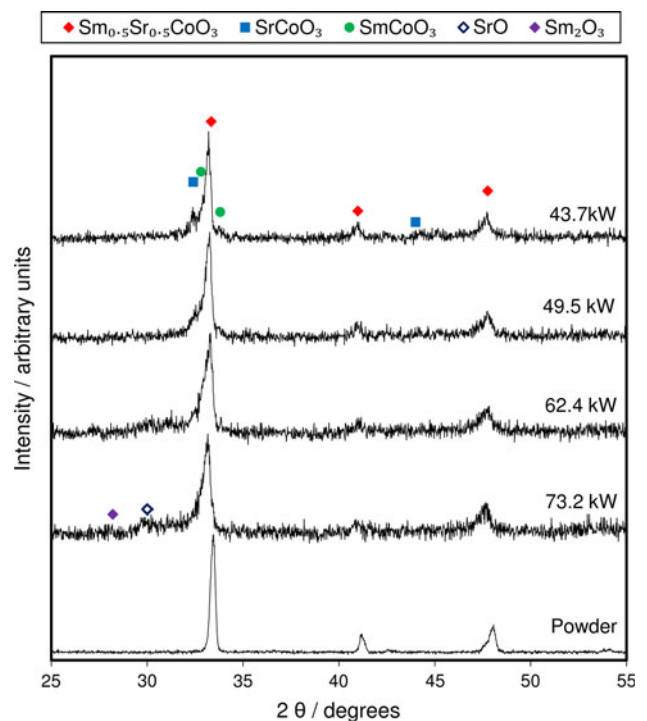


Fig. 6 X-ray diffraction patterns of SSC1000 coatings fabricated with varying plasma power

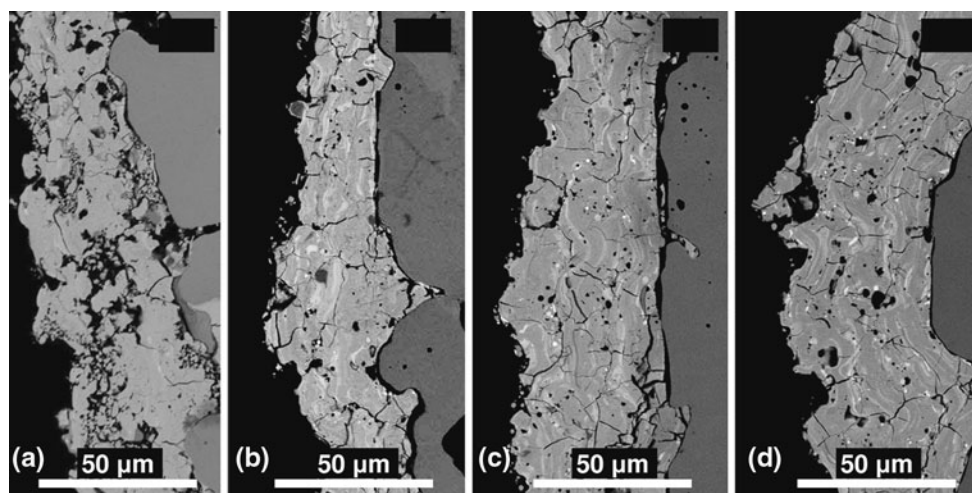


Fig. 7 Cross section micrographs of coatings produced from SSC1000 feedstock with 20, 40, 60, and 80% nitrogen plasmas (balance argon), which resulted in torch powers of 43.7, 53.6, 62.4, and 73.2 kW, respectively

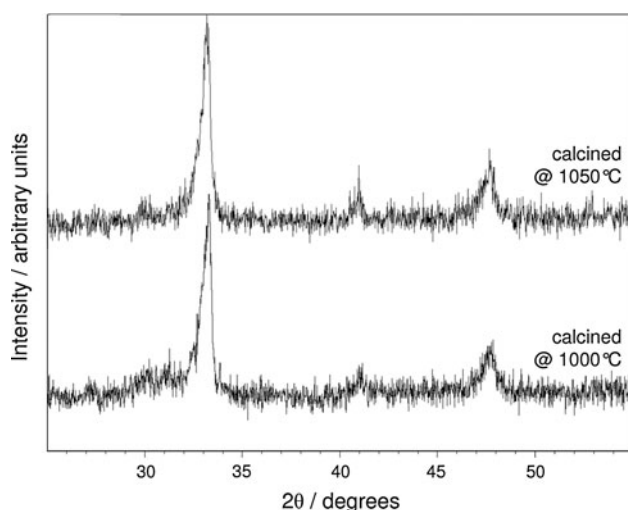


Fig. 8 X-ray diffraction patterns of SSC coatings plasma sprayed from SSC1050 and SSC1000 feedstocks using a 63 kW plasma (60% nitrogen/40% argon)

with 43.7, 53.6, 62.4, and 73.2 kW of power. In these images, there is a contrast in brightness within the bulk of the SSC coatings: this contrast is likely caused by the presence of an undesired phase resulting from decomposed SSC that has a different elemental composition, leading to atomic-number contrast in the backscattered electron SEM images. Markedly, there is greater contrast in images of SSC coatings produced with higher powers than there is in images of coatings produced with lower powers. This observation agrees with the x-ray diffraction results, which show more decomposition when more powerful plasmas are used.

In an attempt to decrease decomposition, SSC coatings were plasma sprayed from a feedstock calcined at a higher temperature, 1050 °C (i.e. SSC1050). Previously, we reported that this strategy decreased decomposition of LSCF in the plasma because the calcination improved the

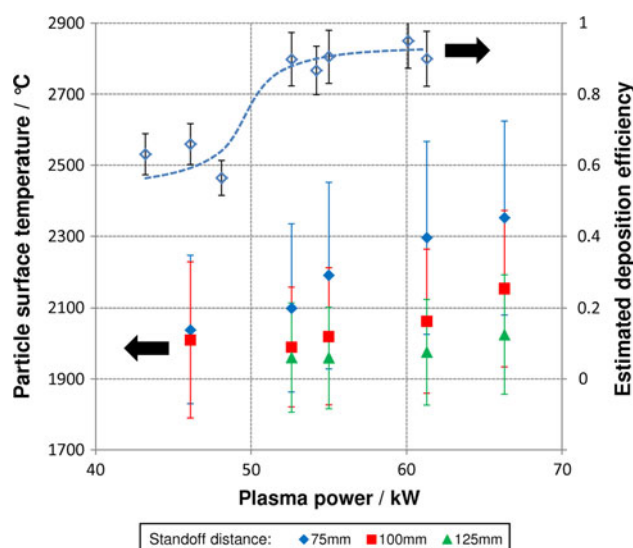


Fig. 9 In-flight temperature measurements and deposition efficiencies of SSC1050

particle cohesion (Ref 10). With SSC, the higher calcination temperature resulted in less decomposition. As seen in Fig. 8, the relative intensity in the $2\theta = 30\text{--}32^\circ$ range, compared to the main perovskite peak intensity, is lower in the coating produced from SSC1050 than in the coating produced from SSC1000 at the same spray conditions.

The in-flight surface temperatures and deposition efficiencies were measured for SSC1050, and they are plotted in Fig. 9. High deposition efficiencies were obtained when the particle surface temperatures were above approximately 2100 °C. The error bars for deposition efficiency account for fluctuations in the powder feed rate and the deceleration of the torch robot during turn-arounds in the raster pattern. The error bars for particle surface temperature represent the standard deviations of the temperature distributions.

Backscattered electron micrographs of three SSC1050 coatings with similar deposition efficiencies are shown in Fig. 10. In Fig. 10(a), there are some small brighter areas in the coating, likely indicating the presence of a secondary phase with different elemental composition from the primary perovskite phase. This undesired phase is likely the result of decomposition, which occurred when the coating was fabricated with a 62.4 kW plasma. This secondary phase is not visually observed in the images of coatings fabricated with 56.6 and 52.9 kW plasmas. Coatings made from less powerful plasmas have higher

porosity; during flight, the feedstock likely melted to a lesser extent in the lower power plasmas, consistent with the lower measured particle surface temperatures.

The average permeation rates from forced flow gas transport measurements are shown in Table 1. As expected, the highest permeation rate was observed in the coating with the highest porosity. However, the coating produced with a 62.4 kW plasma has a fairly high permeation rate, even though the microstructure appears more dense on the micrometre scale. This relatively high permeation rate is most likely due to the large cracks,

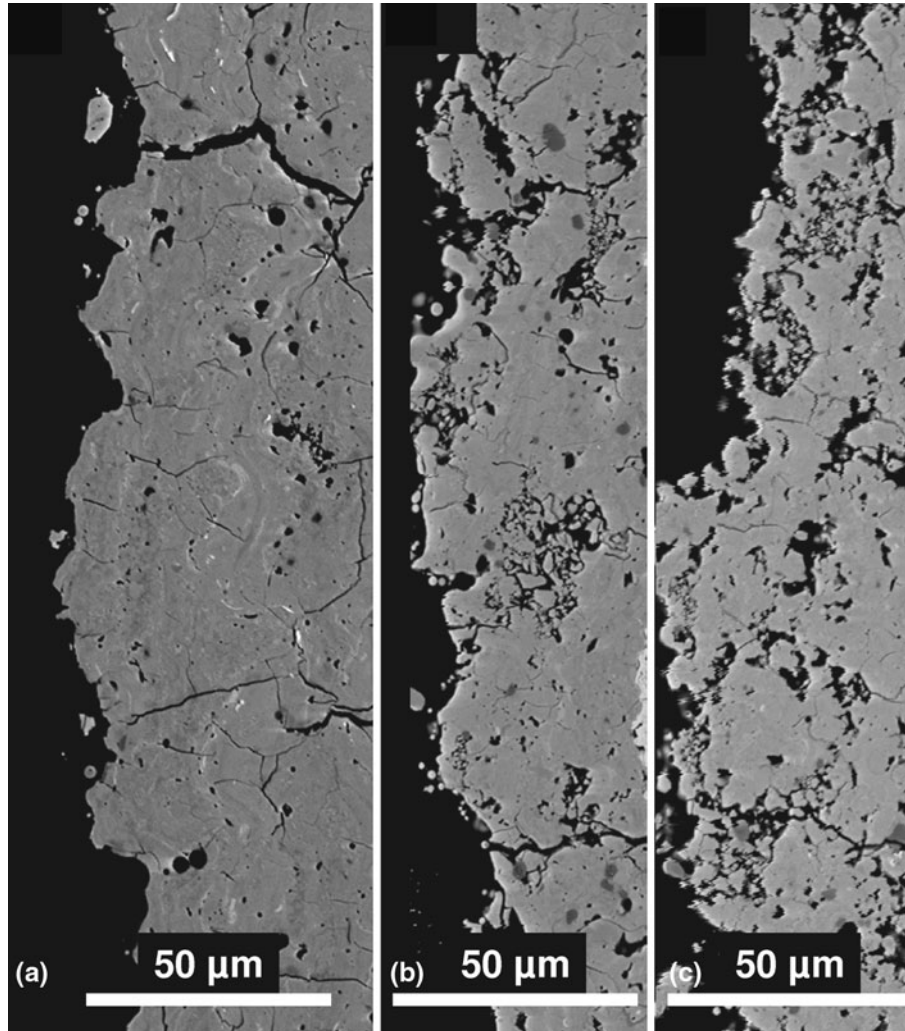


Fig. 10 Cathodes produced from SSC1050 feedstock using (a) 62.4, (b) 56.6, and (c) 52.9 kW plasmas, respectively, corresponding to 50, 40, and 30% nitrogen plasma compositions (balance argon)

Table 1 Properties of SSC1050 cathodes fabricated with various plasma powers

Plasma power, kW	Permeation rate, $\text{sccm/m}^2/\text{kPa}$	Coating thickness, μm	Polarization resistance at 650 °C (Ref 17), $\Omega \text{ cm}^2$
62.4	3.51	72 ± 11	0.521
56.6	2.74	65 ± 14	0.107
52.9	3.82	63 ± 14	0.171

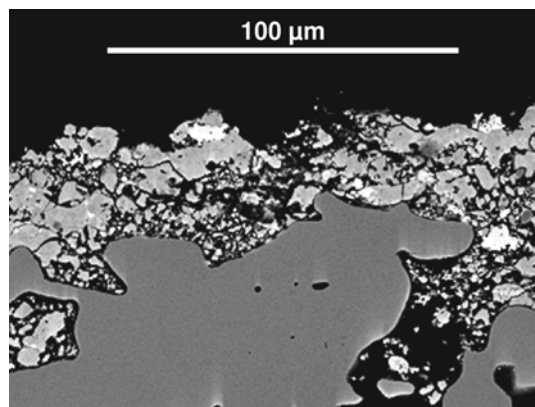


Fig. 11 Composite SSC-SDC cathode

visible in Fig. 10(a), which result from quenching stresses, and which are more prevalent in the coatings that were produced at higher plasma powers. Such a microstructure is undesirable for an SOFC cathode because the electrochemical reaction surface area is low, and the reactions would be concentrated around the large cracks.

Overall, the combination of material decomposition and microstructures that have low porosity make the SSC cathodes produced with 62.4 kW plasmas less desirable than cathodes produced at lower plasma powers. These observations further explain previously reported results (listed in Table 1), which showed that SSC cathodes produced with 62.4 kW plasmas have significantly higher polarization resistances at 650 °C compared to cathodes fabricated with less powerful plasmas (Ref 17).

Composite SSC-SDC cathodes were produced because it has been previously shown that the addition of the SDC phase improves the microstructural stability of the cathode (Ref 14, 15). Two feedstock compositions were used for plasma spraying: one contained 75 wt.% SSC1050 and 25 wt.% SDC, and the other consisted of 60 wt.% SSC1050 and 40 wt.% SDC. Using a low power 52 kW plasma, SDC was incorporated into the coating, as shown in the micrograph in Fig. 11, where the brightest regions correspond to SDC. Deposition efficiencies were 78 and 64% for coatings fabricated from feedstock mixtures containing 25 wt.% SDC and 40 wt.% SDC, respectively. As expected, deposition efficiency decreased with an increase in the amount of SDC in the feedstock because SDC has a significantly higher melting temperature than SSC. The deposition efficiency of SDC can be improved by increasing the particle surface temperature in-flight; however, this increase would require plasmas with higher powers that cause the SSC phase to readily decompose. Thus, the maximum deposition efficiency may be inherently limited when spraying perovskite-fluorite composite coatings, particularly when high porosity and phase purity are important goals.

4. Summary

Single phase and composite cathodes based on LSCF and SSC were manufactured by axial-injection APS. Based on

in-flight temperature measurements, it was found that high deposition efficiencies (>80%) were achieved when sufficient plasma power was used to heat the feedstock particles. An average surface temperature of approximately 2200 °C is needed for adequate melting of LSCF particles, and an average surface temperature of approximately 2100 °C is needed for adequate melting of SSC. On the other hand, excessively high plasma powers produce coarser and denser microstructures, which are undesirable for an SOFC electrode, which requires high gas transport rates and high reaction surface area. Therefore, an optimum plasma power must be selected to produce good microstructures while maintaining high deposition efficiency. For LSCF-SSC composites, the optimum plasma power was found to be 67 kW, and for SSC cathodes, the optimum plasma power was found to be 57 kW. In the case of SSC, high plasma powers can also partially decompose the feedstock, but such decomposition was reduced by calcining the feedstock at a higher temperature. Using a 52 kW plasma, SDC was incorporated into the coatings to produce composite SSC-SDC cathodes.

Acknowledgments

The authors gratefully acknowledge the financial support of the Natural Science and Engineering Research Council of Canada (NSERC) and of Northwest Mettech Corporation.

References

1. F. Tietz, V.A.C. Haanappel, A. Mai, J. Mertens, and D. Stöver, Performance of LSCF Cathodes in Cell Tests, *J. Power Sources*, 2006, **156**, p 20-22
2. E.P. Murray, M.J. Server, and S.A. Barnett, Electrochemical Performance of (La,Sr)(Co,Fe)O₃-(Ce,Gd)O₃ Composite Cathodes, *Solid State Ionics*, 2002, **148**, p 27-34
3. W.G. Wang and M. Mogensen, Solid State Ionics, High-Performance Lanthanum-Ferrite-Based Cathode for SOFC, *Solid State Ionics*, 2005, **176**, p 457-462
4. C. Fu, K. Sun, N. Zhang, X. Chen, and D. Zhou, Electrochemical Characteristics of LSCF-SDC Composite Cathode for Intermediate Temperature SOFC, *Electrochim. Acta*, 2007, **52**, p 4589-4594
5. J. Lagerbom, A. Nikkilä, M. Kylmälahti, P. Vuoristo, U. Kanerva, and T. Varis, Phase Stability and Structure of Conductive Perovskite Ceramic Coatings by Thermal Spraying, *Thermal Spray 2008: Crossing Borders*, E. Lugscheider, Ed., June 2-4, 2008 (Maastricht, The Netherlands), ASM International, 2008, p 1103-1108
6. A.A. Syed, Z. Ilhan, and G. Schiller, Plasma Sprayed Oxygen Electrode for Solid Oxide Fuel Cells and High Temperature Water Heaters, *Thermal Spray 2008: Crossing Borders*, E. Lugscheider, Ed., June 2-4, 2008 (Maastricht, The Netherlands), ASM International, 2008, p 190-194
7. G. Schiller, A. Ansar, M. Lang, and O. Patz, High Temperature Water Electrolysis Using Metal Supported Solid Oxide Electrolyser Cells (SOEC), *J. Appl. Electrochem.*, 2009, **39**, p 293-301
8. A. Ansar, D. Soysal, Z. Ilhan, N. Wagner, S. Wolf, and R. Ruckdaschel, Improving Stoichiometry and Processing of LSCF Oxygen Electrode for SOFC, *ECS Trans.*, 2009, **25**, p 2443-2453
9. A. Ansar, D. Soysal, Z. Ilhan, and N. Wagner, Plasma Sprayed LSCF Oxygen Electrode for SOFC, *Thermal Spray 2010: Global Solutions for Future Applications*, B.R. Marple, Ed., May 3-5, 2010 (Singapore), ASM International, 2010, p 123-128

10. J. Harris and O. Kesler, Atmospheric Plasma Spraying Low-Temperature Cathode Materials for Solid Oxide Fuel Cells, *J. Therm. Spray Technol.*, 2010, **19**, p 328-335
11. J. Harris and O. Kesler, Fabrication of Composite LSCF-SDC Cathode Coatings by Plasma Spray Processing, *ECS Trans.*, 2009, **25**, p 2455-2461
12. C. Xia, W. Rauch, F. Chen, and M. Liu, $\text{Sm}_{0.5}\text{Sr}_{0.5}\text{CoO}_3$ Cathodes for Low-Temperature SOFCs, *Solid State Ionics*, 2002, **149**, p 11-19
13. S. Yang, T. He, and Q. He, $\text{Sm}_{0.5}\text{Sr}_{0.5}\text{CoO}_3$ Cathode Material from Glycine-Nitrate Process: Formation, Characterization, and Application in LaGaO_3 -Based Solid Oxide Fuel Cells, *J. Alloys Compd.*, 2008, **450**, p 400-404
14. X. Zhang, M. Robertson, S. Yick, C. Deces-Petit, E. Styles, W. Ou, Y. Xie, R. Hui, J. Roller, O. Kesler, R. Maric, and D. Ghosh, $\text{Sm}_{0.5}\text{Sr}_{0.5}\text{CoO}_3 + \text{Sm}_{0.2}\text{Ce}_{0.8}\text{O}_{1.9}$ Composite Cathode for Cermet Supported Thin $\text{Sm}_{0.2}\text{Ce}_{0.8}\text{O}_{1.9}$ Electrolyte SOFC Operating Below 600 °C, *J. Power Sources*, 2006, **16**, p 1211-1216
15. X. Zhang, M. Robertson, C. Deces-Petit, and O. Kesler, Composite Cathode Study for Low Temperature SOFC, *ECS Trans.*, 2009, **25**, p 2463-2471
16. X.-M. Wang, C.-X. Li, C.-J. Li, L.-H. Tian, and B. Song, Microstructure and Electrochemical Behavior of $\text{Sm}_{0.5}\text{Sr}_{0.5}\text{CoO}_3$ Deposited by Solution Precursor Plasma Spraying, *Thermal Spray 2010: Global Solutions for Future Applications*, B.R. Marple, Ed., May 3-5, 2010 (Singapore), ASM International, 2010, p 905-909
17. J. Harris and O. Kesler, Performance of Metal-Supported Composite and Single-Phase Cathodes Based on LSCF and SSC, *ECS Trans.*, 2011, **35**, p 1927-1934
18. J. Mager, A. Burgess, R. Pavan, and J. Orzechowski, Thick Aluminum Coating Using Axial Plasma Spray for Proton Beam Collimators, *Thermal Spray 2004: Advances in Technology and Applications*, May 10-12, 2004 (Osaka, Japan), ASM International, 2004, p 76-79
19. J.-G. Legoux, B. Arsenault, L. Leblanc, V. Bouyer, and C. Moreau, Evaluation of Four High Velocity Thermal Spray Guns Using WC-10% Co-4% Cr Cermets, *J. Therm. Spray Technol.*, 2002, **11**, p 86-94
20. B.D. White, O. Kesler, and L. Rose, Air Plasma Spray Processing and Electrochemical Characterization of SOFC Composite Cathodes, *J. Power Sources*, 2008, **178**, p 334-343